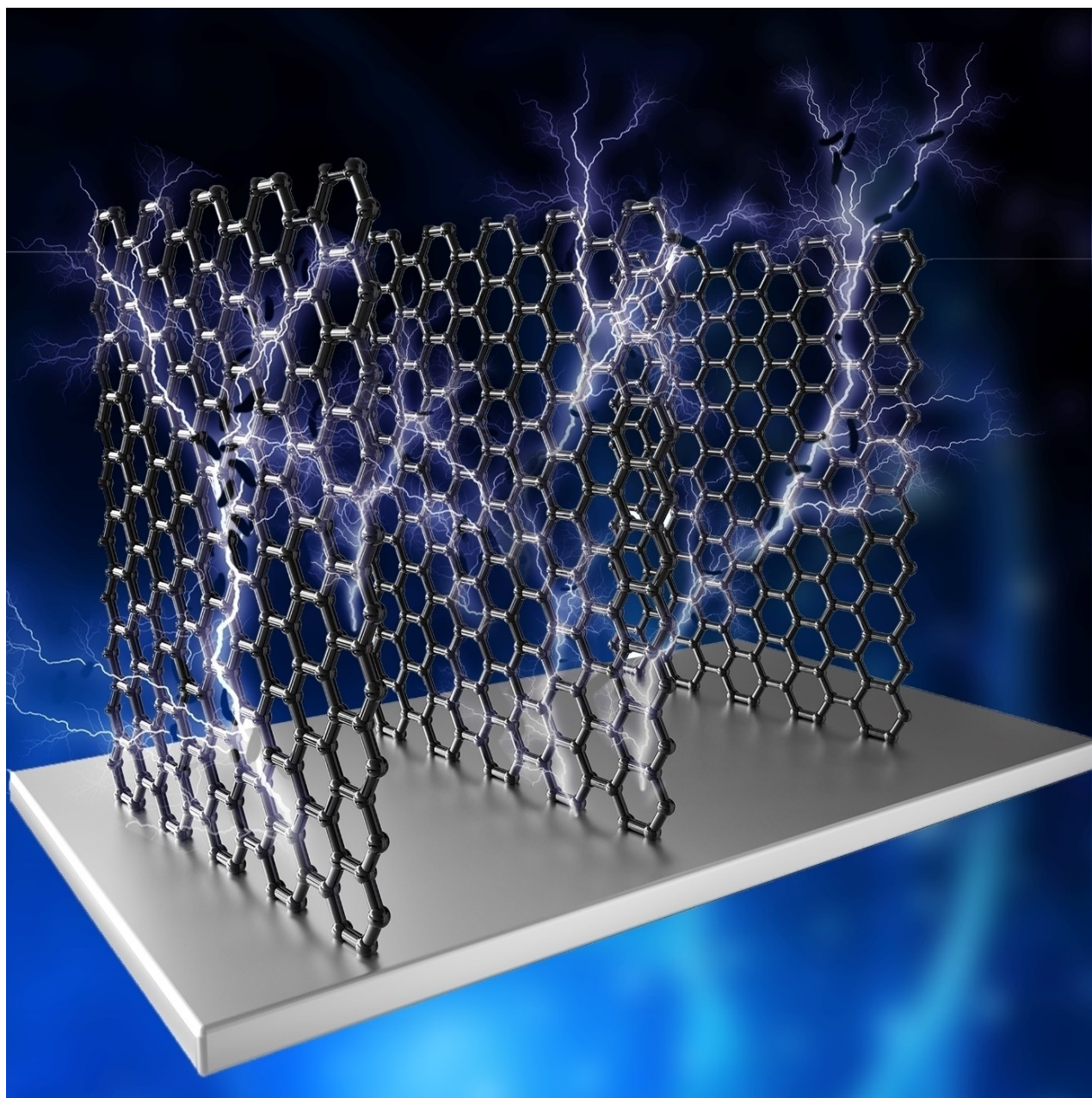


Special
Collection

Vertically Oriented Graphene Nanosheets for Electrochemical Energy Storage

Pingge He^[a, b] and Shaowei Chen^{*[a]}

Vertically oriented graphene (VG) nanosheets exhibit unique structural characteristics, such as large accessible surface area, rich edges, high electrical conductivity, open network channels, and agglomeration resistance, for electrochemical energy-storage applications (e.g., supercapacitors, lithium-ion batteries, etc.). In this Review article, we summarize recent progress in the design and engineering of VG-based electrodes for high-

performance electrochemical energy technologies within the context of energy-storage mechanisms and charge-transfer kinetics, and include a perspective to highlight the challenges and promises in the exploitation of vertically oriented two-dimensional carbon nanostructures for further enhancement of the performance of electrochemical energy-storage devices.

1. Introduction

Graphene, with sp^2 -bonded carbon atoms hexagonally arranged in single-atom thickness, has been attracting extensive attention, due to its unique electronic, mechanical, and thermal properties^[1] and diverse applications in various fields, such as field emission, electronics, sensors, and energy technologies.^[2,3] Among these, graphene has been used extensively as electrode materials for electrochemical energy conversion and storage, thanks largely to its high theoretical specific surface area (up to $2600\text{ m}^2\text{ g}^{-1}$) and electrical conductivity.^[4] In fact, remarkable performance has been achieved with graphene-based supercapacitors and secondary batteries (e.g., lithium-ion battery, sodium-ion battery, etc.).^[5–7] Nevertheless, despite substantial progress in recent years, critical issues remain, as aggregation of graphene nanosheets may occur in practical applications and compromise the device performance, due to a reduced accessible surface area and diminished electron-transfer kinetics.

Conventional graphene materials are horizontally attached (grown) on a substrate (Figure 1a), showing a smooth and flat surface, and when mixed, can easily agglomerate, due to π - π van der Waals interactions between the graphene nanosheets, leading to a reduced active area. By contrast, with a free-standing structure, vertically-grown graphene (VG) nanosheets of a few layers in thickness (Figure 1b) features a large accessible surface area and open channels for effective mass transport of electrolyte ions and reaction species, sharp edges for adsorption of reaction intermediates and fast electron transfer,^[8] and resistance against agglomeration. These characteristics are conducive to facile electron-transfer reactions in electrochemical energy storage technologies.

In this review, we will summarize recent progress in the synthesis and applications of VG in contemporary electrochemical energy storage technologies, with a focus on the mechanistic origin of the growth and electron-transfer dynamics of the materials. A perspective is also included to highlight

the potential of two-dimensional carbon nanostructures in the development of high-performance electrochemical energy storage systems.

2. Unique Morphology and Properties

VG, standing vertically on a substrate, typically consists of a few graphene layers and exhibit sharp edges and a high aspect ratio (Figure 2a–c), corresponding to a thickness from a few to a few tens of nanometers (Figure 2d).^[9–11] A variety of substrates have been used for the growth of VG, such as carbon cloth (Figure 2a),^[9] Ni foam (Figure 2b),^[10] Si (Figure 2c) and SiO_2 ,^[11] which show virtually no influence on the morphology of the

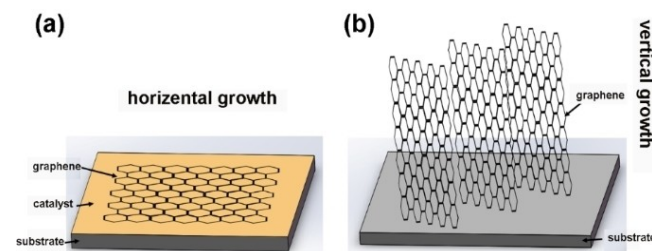


Figure 1. Schematic illustrations of graphene nanosheets by a) conventional horizontal growth and b) vertical growth.

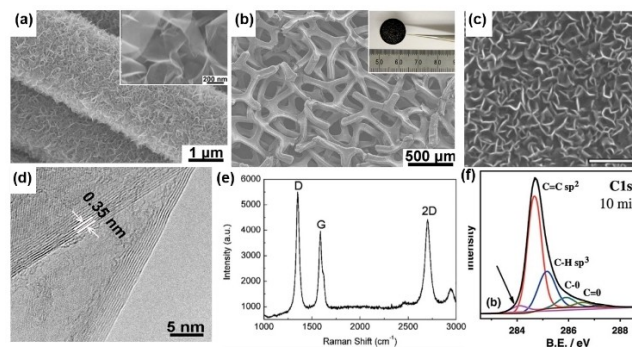



Figure 2. SEM images of VG grown on a) carbon cloth (reproduced with permission from Ref. [9]; copyright 2015, Royal Society of Chemistry); b) Ni foam (reproduced with permission from Ref. [10]; copyright 2016, Wiley-VCH); and c) Si (scale bar 400 nm, reproduced with permission from Ref. [11]; copyright 2016, Elsevier). d) TEM image (reproduced with permission from Ref. [9]; copyright 2015, Royal Society of Chemistry); e) Raman spectrum (reproduced with permission from Ref. [11]; copyright 2016, Elsevier) and f) C 1s XPS spectrum of VG with a growth time of 10 min (reproduced with permission from Ref. [18]; copyright 2014, Wiley-VCH). Inset to panel (a) is a magnified SEM image and inset to panel (b) is a photograph of the resulting VG.

[a] Dr. P. He, Prof. S. Chen
 Department of Chemistry and Biochemistry
 University of California
 1156 High Street, Santa Cruz, California 95064, USA
 E-mail: shaowei@ucsc.edu

[b] Dr. P. He
 Institute of Advanced Materials and Technology
 University of Science and Technology Beijing
 30 Xueyuan Road, Beijing 100083, China

 An invited contribution to a joint Special Collection between ChemElectroChem and Batteries & Supercaps dedicated to research Beyond Lithium-Ion Batteries

final VG products. In Raman measurements, several characteristic vibrational bands of VG can be readily identified at ca. 1350 cm^{-1} (D band), 1585 cm^{-1} (G band), and 2700 cm^{-1} (2D band). The D band originates from the disordered structure of VG, such as the random orientation of crystalline carbon,^[12,13] out-of-plane defects,^[14] and fullerene-like structures,^[15] the G band is due to the sp^2 -hybridized carbon in the graphitic planes,^[16] and the position and shape of the 2D peak are correlated to the number of the graphene nanosheet layers.^[17] That is, the high intensity of the D and 2D bands signifies abundant defects in the graphene nanosheets, and vice versa (Figure 2e).^[11] This can be further confirmed by results from X-ray photoelectron spectroscopy (XPS) measurements, where sp^2 and sp^3 hybridized carbon can be readily resolved and quantified (Figure 2f).^[18]

With such unique morphologies, VG exhibits distinctive features, as compared to conventional horizontally-grown graphene nanosheets.^[19] First, VG shows a large specific surface area and is less prone to stacking/aggregation than the horizontally grown counterparts. Second, VG possesses open channels between the nanosheets making the entire surface area accessible by electrolyte ions in electrochemical applications, as the spacing between adjacent VG nanosheets ranges from a few tens to several hundred nanometers.^[20,21] In fact, the specific surface area of VG can be as high as $1100\text{ m}^2\text{ g}^{-1}$.^[22] Besides, the exposed thin edges of VG provide abundant active sites for ion/charge absorption/desorption, a critical step in electrochemical reactions. An individual VG nanosheet typically shows a tapered shape, with a few graphene layers formed at the base and atomically thin carbon layers at the top. Such sharp edges have been demonstrated to significantly concentrate charge density during charge/discharge processes, leading to enhanced energy storage capacity.^[23] Third, VG nanosheets can act as strengthening ribs, remarkably improving mechanical performance.^[24] Individual VG nanosheets have been used as free-standing and self-support walls, which effectively stand up against the van der Waals interactions between nanosheets and prevent collapsing and stacking with each other in random directions, leading to enhanced mechanical strength.

3. Synthesis and Characterizations

3.1. Synthetic Methods

Great efforts have been devoted to controllable and effective preparation of VG in high quality, and plasma-coupled chemical vapor deposition (CVD) has been the most widely used technique, which can be operated at low reaction temperatures, and without the need of a catalyst. The method can be further classified according to the plasma sources, such as microwave plasma,^[25,26] radio frequency (RF) inductively coupled plasma (ICP),^[20] RF capacitively coupled plasma (CCP) assisted by hydrogen radical injection,^[27,28] DC plasma,^[29] helicon-wave plasma,^[30] and electron beam excited plasma (EBEP).^[31] Among them, microwave plasma, RF-ICP, and EBEP-based CVD methods have been highly developed for the fabrication of VG.

Thanks to its high intensity, microwave plasma can be used for decomposing H_2 molecules to generate H atoms effectively.^[19] As shown in Figure 3, a microwave (2.45 GHz) is coupled from the rectangular waveguide into the cavity via an axial antenna. A discharge called a "plasma ball" is generated above the substrate, and heats the substrate. In this system, the CVD process is operated at relatively low pressures of a few tens of Torr. However, at too high a pressure or too low a microwave power, plasma cannot be sustained. If the microwave power is too high for a given pressure, the plasma becomes unstable and tends to jump to the quartz (fused silica) window, occasionally resulting in the destruction of the window by the heat.^[19]

RF-ICP (13.56 MHz) has been used to etch a range of materials, such as Si, SiO_x , SiN_x , and metal films, in a large-scale integration fabrication process. The ICP is operated at relatively low pressures below 100 mTorr (13.3 Pa). The plasma is contained inside a chamber, which is surrounded by an inductive coil antenna. There are two types of ICP geometries: planar and cylindrical. In the planar geometry, the electrode is a coil antenna of the flat metal wound like a spiral, and in the cylindrical geometry, it is like a helical spring.^[32] An RF-ICP CVD system has the advantages of simple design and scalability for large area growth. Notably, the growth rate of carbon nano-



Pingge He received her B.S. and Ph.D. degrees in Materials Science and Engineering from Central South University (China) in 2012 and 2017, respectively. During her Ph.D. study, she visited the Birck Nanotechnology Center of Purdue University (USA) from 2014 to 2017. After that, she was appointed as an Associate Professor at the University of Science and Technology Beijing (China) in 2018. Currently, she is doing her postdoctoral research in Prof. Chen's group at the University of California-Santa Cruz (UCSC, USA), and her research work has been focused on carbon nanostructures and applications in electrochemical energy-storage and electrocatalysis.



Shaowei Chen received his B.S. degree in Chemistry from the University of Science and Technology of China in 1991, and M.S. and Ph.D. degrees from Cornell University (USA) in 1993 and 1996, respectively. Following a postdoctoral appointment at the University of North Carolina – Chapel Hill (USA), he started his independent career in Southern Illinois University (USA) in 1998. He moved to UCSC (USA) in 2004 and is currently a Professor of Chemistry and the Faculty Director of the UCSC COSMOS program. His research is primarily focused on the electron-transfer chemistry of functional nanomaterials, and applications in electrocatalysis and antimicrobials.

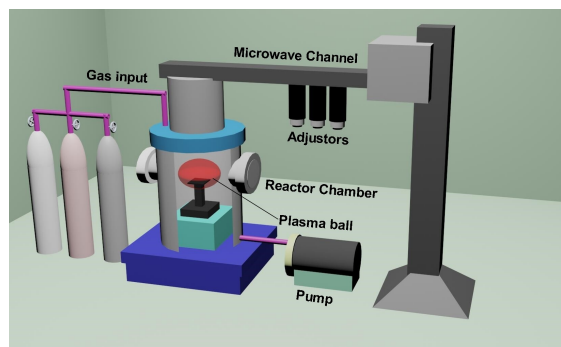


Figure 3. Schematic illustration of a microwave plasma CVD instrument.

walls using RF-ICP CVD with a CH_4/Ar mixture can be rather high, as compared to other methods.^[19]

EBEP is a high-intensity plasma directly introduced by a high-current and low-energy electron beam.^[19,33] The electron-beam energy and electron current can be controlled independently by changing the accelerating voltage and discharge current, respectively. When the electron beam energy is close to the energy corresponding to the maximum electron impact ionization cross-section of the source gases, highly ionized and dissociated plasmas can be produced even at low pressures. Generally, VG sheets fabricated by the EBEP-CVD with CH_4/H_2 can be easily detached from the substrate, and such isolated free-standing VG can be used for the fabrication of novel electronic devices.^[33]

3.2. Characterization Methods

Effective characterization methods are essential to unravel the microstructures of VG and distinguish VG from other carbon nanostructures. These include the conventional characterization tools of X-ray diffraction (XRD), XPS, scanning electron microscopy (SEM), transmission electron microscopy (TEM), and Raman spectroscopy.

SEM is a direct way to visualize the morphology and orientation of VG (Figure 2a–c). VG grown on conductive substrates can be directly used as SEM samples, where the sharp edge of VG can be distinguished based on the contrast depth. The number of layers of the VG edges can be quantified by TEM measurements based on an accurate assessment of the thickness (Figure 2d). Further structural insights can be obtained from XRD and selected area electron diffraction (SAED) measurements, where the hexagonal patterns of the graphene crystal structure can be readily identified. Raman spectroscopy is a quick and effective way for structural characterization and quality control of VG (Figure 2e), based on a careful analysis and comparison of the vibrational energy and intensity of the D, G, and 2D bands (Figure 2e).^[17] These results can then be correlated with the carbon atoms in different chemical structures, as resolved in XPS measurements (Figure 2f).

Experimentally, these characterization methods are usually combined to yield a holistic picture of the VG microstructures, a

key step towards the correlation between VG structure and electrochemical performance.

4. Growth Mechanism

Although various methods have been adopted to prepare VG, the growth mechanism remains elusive,^[34] limiting further development of VG in practical applications. Different from conventional CVD for horizontal graphene growth, plasma-based CVD shows a more complicated growth process, and numerous factors, such as plasma source, plasma power, carbon source, etc., may impact the VG's growth dynamics. Generally, the growth process involves three steps: nucleation, vertical growth, and saturation: (i) a buffer layer is formed on the substrate surface with irregular cracks and dangling bonds, where vertical nanosheets preferentially grow; (ii) with an increase of the growth time, both the spacing between the nanosheets at the top (forming open edges) and the nanosheet size increase gradually; and (iii) due to the balance between material deposition and etching effects by the plasma, the growth process becomes saturated, resulting in the formation of two-dimensional carbon nanosheets standing vertically on the substrate with a high aspect ratio.^[35]

4.1. Nucleation

Nucleation is an important first step in VG growth. Studies have demonstrated that a thin carbon film formed on the substrate surface will act as nucleation sites for VG growth,^[36] and the upward curling force leads to the takeoff of some top carbon layers at the grain boundaries that continue to grow perpendicularly to the substrate.^[37] In a previous study,^[11] Zhang *et al.* proposed a defect-guided mechanism of VG growth, whereby a buffer layer was formed parallel to the substrate surface, and defects propagated with nucleation of VG stemming preferentially from the defects (Figure 4a). It was shown that defects on the buffer layers promoted the growth of VG nanosheets, due to the high activity (Figure 4b–c). Reifenberger *et al.*^[38] showed that carbon deposits firstly formed nanoislands (Figure 4d), which were thought to be the nucleation sites of VG on Si substrates. Rummeli *et al.*^[39] demonstrated that the nucleation of VG growth was either from the buffer layer or the surface of carbon onions. The buffer layer was composed of amorphous and graphitic carbon on the surface with some mismatches (Figure 4e). In contrast, the upper layer of VG nucleated from the carbon onions (Figure 4f). Similar to the buffer layer, the onions also serve as active nucleation sites for VG growth. The graphene layers then grow in the tangential direction, naturally leading to a flower-shaped VG structure. Moreover, as shown in Figure 4g, in a plasma-enhanced CVD with H radical injection employing a $\text{C}_2\text{F}_6/\text{H}_2$ mixture, the height of VG grown on a Si substrate increased linearly with the growth time within the range of 5 to 60 min,^[40] indicating a steady-state growth process. However, in the earlier stage (<5 min), the height of

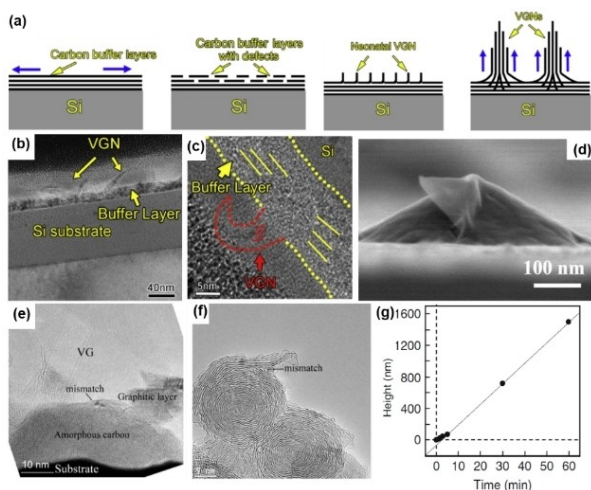


Figure 4. a) Schematic illustration of VG growth. b) Side-view TEM image of VG (buffer layer) on Si substrate. c) HRTEM image of the interface between Si and VG (reproduced with permission from Ref. [11]; copyright 2016, Elsevier). d) Nanoisland nucleation sites for VG growth (reproduced with permission from Ref. [38]; copyright 2012, Elsevier). e) HRTEM image of the buffer layer composed of amorphous carbon and graphitic layer. f) HRTEM image of carbon onion (reproduced with permission from Ref. [39]; copyright 2014, American Chemical Society). g) Height of VGs as a function of growth time (reproduced with permission from Ref. [40]; copyright 2009, American Institute of Physics).

VG exhibited nonlinear dependence on time, indicating a more complicated growth dynamics during the nucleation process.

These various theories are generally based on defects-derived formation mechanism that at the nucleation stage, carbon species are condensed to form nanoislands (buffer layers) with dangling bonds. At these dangling bonds, disordered carbon nanosheets of small sizes are then nucleated, followed by the two-dimensional growth and subsequent formation of graphene nanosheets.

4.2. Vertical Growth

After nucleation sites are formed on the substrate, graphene nanosheets start to grow. As shown in Figure 5a, similar to the growth of 1D carbon nanotubes which follows either the top or bottom mode, vertical 2D growth has several possibilities: at the top edge, on the surface (in the lateral direction), or at the

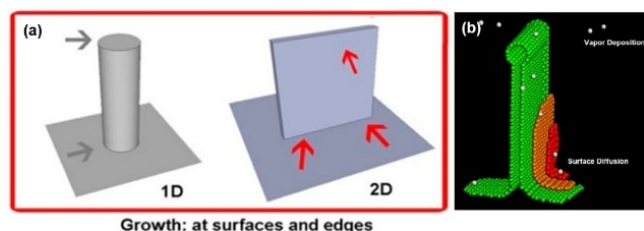


Figure 5. a) Schemes of the growth of 1D and 2D nanostructures where the arrows represent the mass supply for growth. b) A continuum model based on the surface diffusion and moving boundary (reproduced with permission from Ref. [39]; copyright 2014, American Chemical Society).

bottom. During this growth process, a continuum model based on surface diffusion and moving boundary (mass flow) has been developed to describe the intermediate states of the steps and edges of graphene (Figure 5b), and these steps near the top edge have often been observed in various studies.^[39]

Meanwhile, several factors, e.g., electric field, internal stress, and anisotropic growth, have been found to significantly impact the vertical growth of VG.^[8] Specifically, the electric field can produce a relatively large chemical-potential gradient near the surface, due to ion focusing effects and fast delivery of precursors.^[8,39] Meanwhile, during the growth process, as the electrical field is normal to the (conductive) substrate surface and is stronger near the edges and sharp points than in other areas, the localized electric field above the substrate can control the density and orientation of the VG networks.^[41] Another important factor is the internal stress that arises from the temperature gradient, ion bombardment, and lattice mismatch between the substrate and graphene materials, which may become a driving force for VG growth.^[35] Moreover, the directional growth of VG can also be attributed to the anisotropic growth effect. The growth rates in the directions that are parallel and perpendicular to the graphene layer have been demonstrated to be different.^[21] Among the nucleated graphene sheets with random orientations, those standing almost vertically on the substrate surface continue to grow preferentially, owing to the difference in the growth rates along the strongly bonded planes of graphene sheets and the weakly bonded stacking direction. Reactive carbon species arriving at the edge of the graphene layer are easily bonded to the edge, and eventually, the graphene layer will expand preferentially along the direction of radical diffusion, perpendicular to the substrate plane.^[19]

During the vertical growth stage, the height of VG is usually in a positive correlation with the experimental time, and the growth rate is constant, indicating a steady-state process.

4.3. Saturation

Due to the competition between carbon deposition and plasma etching, the growth process will reach saturation. In this stage, the height of VG remains largely unchanged with the increase of time, indicating the completion of VG growth. The closure of open edges determines the final size of the vertical graphene and together with the overall curvature provides the necessary mechanical support for vertical alignment.

5. Applications in Electrochemical Energy-Storage Systems

5.1. Supercapacitors

Supercapacitors are promising energy storage systems in diverse applications, due to their high power density, desirable rate capability, and outstanding cyclic stability.^[42] According to

different energy storage mechanisms, supercapacitors are typically classified into electrical double-layer capacitors (EDLC) and pseudocapacitors. EDLC stores energy from the accumulation of charges at the electrode/electrolyte interface, whereas the pseudocapacitance originates from faradaic reactions occurring at the electrode surface.^[43]

5.1.1. VG-Based Carbon Electrodes for EDLCs

Because of a large specific surface area, high electrical conductivity, open network structure, and robust chemical stability in the electrolyte, VG is promising electrode material for EDLCs. Compared to conventional horizontally grown graphene, VG is less prone to aggregation and exhibits more active sites, due to the sharp edges. Bare VG as binder-free EDLC electrodes can exhibit a high specific capacitance up to 230 Fg^{-1} (at the scan rate of 10 mVs^{-1}) and high areal capacitance of 8.4 mFcm^{-2} at the scan rate of 10 mVs^{-1} .^[44] Notably, the simulated current-voltage curves for the different types of electrodes (vertical, horizontal graphene, and bulk graphite, with the respective models shown in Figure 6a–c, respectively) indicate that the VG electrode exhibits the largest current density (Figure 6d). As shown in Figure 6e, VG entails open channels for facile ion exchange with the shortest straight path, while ions need to pass a more complicated pathway to access the bottom of horizontal graphene. Thus, VG-based electrodes are conducive to ion/charge transfer during the charge/discharge process, and hence a high electrochemical performance.

The interfacial structure and capacitive behaviors of VG edges with representative interlayer spacing have also been studied via molecular dynamics (MD) simulations.^[45] Compared with planar graphite surfaces, edges exhibit a two-fold increase in specific capacitance at a wider interlayer spacing of $\sim 5.0 \text{ \AA}$. Interestingly, a similar screening effect and thickness of the electrical double-layer was observed at the edges with a variety of electrolyte ions. Yet, water molecules can counterbalance the interfacial electrical field more effectively at the edge sites than

on planar graphite surface. This enhanced screening efficiency by water molecules on the edges significantly reduces the total electrical potentials, corroborating the observed capacitance enhancement at edge sites.

To further improve the capacitance of VG electrodes, activation treatments, such as oxidation, plasma treatment, and doping, have been conducted to tune the intrinsic hydrophobicity of VG. Simple oxidation using strong acid/alkali oxidizing agents can improve the wettability of VG.^[46] As shown in Figure 7a, after KOH treatment, ultrathin nanosheets and nanopores were generated on the VG surface, mainly due to the exfoliation of VG sheets during the oxidation process. Moreover, the water contact angle had significantly decreased after KOH treatment (Figure 7b–7c), indicating improved wettability of treated VG. Additionally, Sahoo *et al.*^[47] observed that oxygen-plasma treatments of VG remarkably enhanced the wettability, with the water contact angle decreasing to 0° (Figure 7d–7e). Moreover, the contents of hydroxyl and carbonyl functional groups on VG increased with increasing plasma powers. Electrochemically, plasma-treated VG electrodes showed a much higher areal capacitance (ten times higher), compared to the pristine ones (Figure 7f). Notably, a high degree of oxidation of VG might deteriorate the electrical conductivity, leading to poor rate capability and cyclic stability of the electrodes. Thus, the electrochemical performance of oxidized VG should be optimized by striking a delicate balance between hydrophilicity and electrical conductivity of the materials.

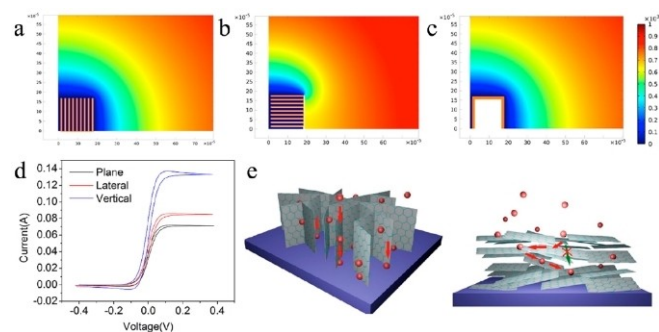


Figure 6. 2D cross-section characteristic concentration profiles of a) vertical electrodes, b) horizontal electrodes, and c) bulk electrodes. d) Simulation of current-voltage curves for the three different electrodes. e) Schematic illustration of ion diffusion direction based on two kinds of graphene electrodes. (reproduced with permission from Ref. [44], copyright 2016, American Chemical Society).

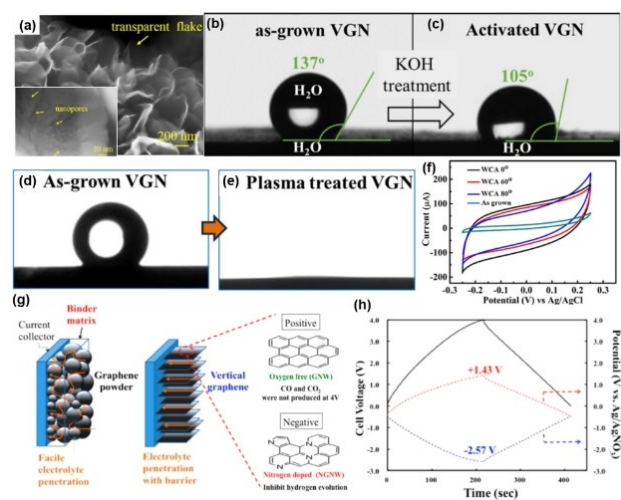


Figure 7. KOH treatment on VG: a) SEM image of VG after KOH treatment. Inset is an SEM image showing the nanopores generated on the VG surface. Water contact angle of b) original and c) KOH-activated VG. (reproduced with permission from Ref. [46]; copyright 2017, American Institute of Physics). Water contact angle of d) original and e) plasma-treated VG. f) CV curves of different VG samples at a scan rate of 100 mVs^{-1} (reproduced with permission from Ref. [47]; copyright 2018, Elsevier). g) Schematic illustration of an active carbon powder-coated electrode and a VG-coated electrode (right-top is the structure of the positive electrode and right-down is the structure of the negative electrode). h) Charge/discharge curves of the positive electrode (red curve), negative electrode (blue curve), and asymmetric device (black curve) (reproduced with permission from Ref. [48]; copyright 2016, American Chemical Society).

Also, doping is an effective way to manipulate the intrinsic property of carbon-based EDLC electrodes. Hu *et al.*^[48] prepared N-doped VG electrodes through a plasma-enhanced CVD process using a mixed flow of CH₄ and N₂, and constructed an asymmetric supercapacitor based on a VG positive electrode and an N-doped VG negative electrode (in 1 M tetraethylammonium tetrafluoroborate/propylene carbonate (TEABF₄/PC) electrolyte) (Figure 7g). In such an asymmetric cell, nitrogen doping significantly suppressed the irreversible reduction of residual water and organic electrolyte at the negative potential end, consequently widening the negative potential window (Figure 7h), and the binder-free VG without oxygen-containing functional groups was inert to the irreversible oxidation of organic electrolytes, resulting in an even wider working potential window. As a result, the as-prepared asymmetric supercapacitor exhibited a cell voltage up to 4 V, high energy density (52 Wh kg⁻¹), high power density (8 kW kg⁻¹), and outstanding cyclic stability (with approximately 100% capacitance retention after 10000 cycles), effectively mitigating the critical issues of low working voltage and energy density of conventional supercapacitors.

Other structural factors, such as the mass ratio of the positive and negative electrodes,^[49] impurity in the electrolyte,^[50] and electrolyte wettability,^[51] have also been demonstrated to show a significant influence on the charge-storage capacity of VG electrodes.

The electrochemical performance can be further enhanced by using all-carbon composite electrodes with VG in combination with other carbon nanostructures of large specific surface areas and appropriate porosity. In these composite electrodes, VG can significantly increase the mechanical strength and surface area of 3D or arrayed carbon nanostructures, making such all-carbon materials feasible in practical applications. For example, for 3D graphene aerogel (GA)^[24] and carbon nanotube (CNT) micro-conduit arrays^[23] that generally show a large specific surface but poor mechanical strength, the incorporation of VG can significantly improve the structural stability and electrochemical performance. In a previous study, using a microwave plasma CVD method, VG was uniformly grown on a substrate (GA or CNT) surface (Figure 8a–c). Importantly, the deposition of VG on GA (Figure 8a) significantly enhanced the mechanical strength (Figure 8d), where VG acted as stiffening ribs layered over the thin cellular sheets within the GA (Figure 8e) and concurrently rendered a uniform stress distribution (Figure 8f), leading to over seven-times improvement in compression strength, as compared to pristine GA. Thus, the obtained free-standing and binder-free VG/GA electrode exhibited a high specific capacitance of 245 F g⁻¹ (based on the entire electrode mass), which corresponded to a high areal capacitance of 1.1 F cm⁻², desirable rate capability, and outstanding cyclic stability with capacitance retention of 92% after 10000 cycles.^[24]

Deposition of VG on CNT also significantly enhanced the mechanical strength and structural stability of such all-carbon electrodes (inset to Figure 8g), leading to a markedly increased specific capacitance (ca. 500 F g⁻¹, Figure 8g) and outstanding cycle life (capacitance retention of ca. 95% over 10000 cycles).

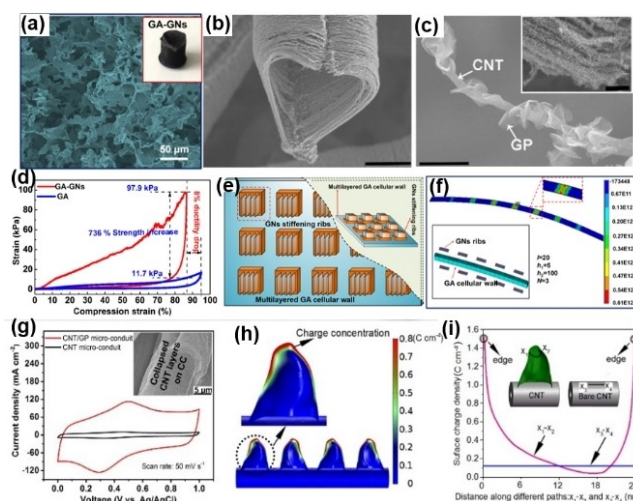


Figure 8. SEM images of a) VG grown on GA. Inset is a photograph of the VG/GA sample (reproduced with permission from Ref. [24]; copyright 2018, Elsevier). b) VG grown on CNT micro-conduit. c) VG uniformly grown on a single CNT surface. Inset is an SEM image showing the dense and homogenous coverage. (reproduced with permission from Ref. [23]; copyright 2018, Nature). d) Mechanical properties of bare GA and VG/GA. e) Schematic model of finite element simulation for the mechanical strengthening mechanism of VG layered over GA templates. f) Stress mapping analysis of a cellular wall within a GA-GN structure. (reproduced with permission from Ref. [24]; copyright 2018, Elsevier). g) CV curves of VG/CNT/CC and CNT/CC electrodes, and inset is an SEM image of the bare CNT arrays after immersion into the electrolyte. h) Simulated charge concentration distribution on VG and CNT. i) Calculated surface charge density of VG/CNT. (reproduced with permission from Ref. [23]; copyright 2018, Nature).

Importantly, as shown in Figure 8h, results from density functional theory (DFT) calculations suggested that during the charge/discharge process, charges/ions were concentrated at the edge region of VG, resulting in a much higher (almost eight times) surface charge density in the edge region than that in the basal region, and the surface charge density of VG was also much higher than that of CNT (Figure 8i), suggesting that the edges of VG were responsible for the outstanding electrochemical performance of such all-carbon electrodes.^[23]

In short, whereas traditional carbon-based EDLC electrodes usually suffer low capacitance, the introduction of VG can lead to significant enhancement of the surface area and mechanical stability (structural stability), and consequently a markedly improved electrochemical performance. Nevertheless, further improvement is desired, in particular, with regards to the work voltage and capacity of VG-based carbon electrodes for supercapacitors. Loading pseudocapacitive materials on VG represents a unique strategy to increase the capacity of the electrodes, as detailed below.

5.1.2. VG-Based Hybrid Electrodes for Pseudocapacitors

VG with a large specific surface area and high electrical conductivity also shows great promise as structural scaffolds for the deposition of pseudocapacitive materials, e.g., metal oxides/hydroxides and conducting polymers, to ameliorate the charge transfer efficiency and further enhance the structural

stability of the electrodes. MnO_2 has been one of the most widely used pseudocapacitive electrode materials, due to its rapid redox kinetics, wide operating voltage, and low cost,^[52] which shows great promise to composite with VG as high-performance hybrid electrodes. The direct reaction of VG with KMnO_4 is the most common method in the preparation of MnO_2/VG composites. In this reaction, the VG (carbon) substrate acts as a sacrificial reductant, and meanwhile, aqueous permanganate is converted to insoluble MnO_2 , which is deposited onto the surface of VG. Fisher *et al.*^[53] prepared a hybrid electrode with a uniform coverage of MnO_2 on the VG surface, and observed a high specific capacitance of 580 F g^{-1} in $1 \text{ M Na}_2\text{SO}_4$ aqueous electrolyte. In such a hybrid electrode, VG entailed conductive channels to facilitate charge transfer at the VG/ MnO_2 interface, leading to a low interfacial resistance and high cyclic stability of the hybrid electrodes. Moreover, MnO_2 nanosheets can be grown on the VG surface through a facile electrodeposition process.^[54] The performance of the as-prepared MnO_2/VG composite electrodes could be optimized by adjusting the electrodeposition time, reaching a high specific capacitance of 565.32 F g^{-1} at a current density of 1 A g^{-1} . Besides MnO_2 , other metal oxides, such as RuO_2 ,^[55] Co_3O_4 ,^[56] and TiO_2 ,^[57] have also been investigated as active materials to combine with VG as hybrid electrodes. For instance, an all-solid-state symmetric supercapacitor was fabricated based on Co_3O_4 nanoparticle/VG hybrid electrodes.^[56] The VG served as an excellent backbone, together with the carbon fabric, and the as-prepared composite electrodes showed an ultrahigh specific capacitance of 3480 F g^{-1} , approaching the theoretical value of Co_3O_4 (3560 F g^{-1}). As a result, an all-solid-state symmetric supercapacitor device based on such composite electrodes delivered a high capacitance (580 F g^{-1}), good cycling ability (86.2% capacitance retention after 20000 cycles), high energy density (80 Wh kg^{-1}), and high power-density (20 kW kg^{-1} at 27 Wh kg^{-1}).

Compared to metal oxides,^[58] metal hydroxides generally show higher electrochemical activity, but lower conductivity and structural stability severely limit their wide applications in supercapacitors. Thus, VG has been employed as substrates for metal hydroxides of various nanostructures (Figure 9a) to effectively facilitate charge transfer and improve the structural stability of the hybrid electrodes. For instance, Zheng *et al.*^[59] prepared a hybrid electrode with $\text{Ni}(\text{OH})_2$ nanosheets electrodeposited on a VG surface (supported on Ni foam). The introduction of VG led to the dense growth of nanocrystalline $\beta\text{-Ni}(\text{OH})_2$, and the hybrid electrode exhibited a high specific capacitance of 2215 F g^{-1} , improved cycling stability, and high rate capability.

To further improve the electrical conductivity and electrochemical activity of metal hydroxides, binary (e.g., Ni–Co hydroxide, Ni–Mn hydroxide) or multi-component metal hydroxides have been used. For instance, binary Ni–Co hydroxide nanosheets have been electrodeposited on the VG foam surface to prepare a hybrid electrode (Figure 9b).^[10] The hierarchical structure with smaller Ni–Co hydroxide nanosheets on larger VG endowed the lightweight hybrid electrode with an ultrahigh volumetric capacitance of 765 F cm^{-3} , which was the highest

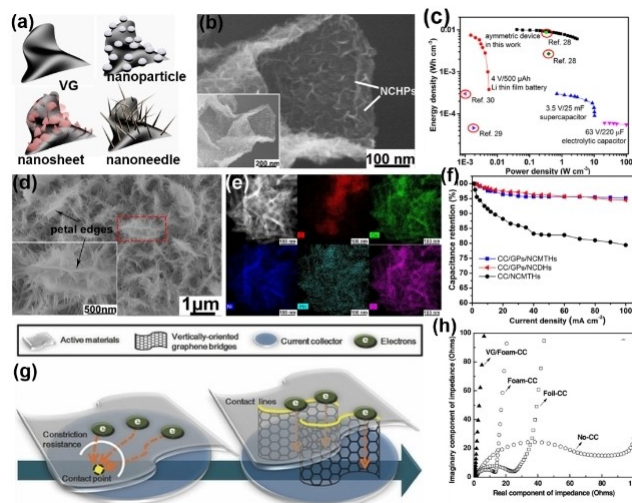


Figure 9. a) Scheme of metal hydroxides with various nanostructures on VG. b) SEM images of a uniform distribution of Ni–Co hydroxide nanosheets on the VG surface. Inset is the close-up view of the VG surface. c) Ragone plot of an asymmetric device compared to other contemporary cells. (reproduced with permission from Ref. [10]; copyright 2016, Wiley-VCH). d) Ni–Co–Mn hydroxide nanoneedles deposited on the VG surface. Inset is an enlarged SEM image showing the sharp edge of VGs. e) EDX-based elemental maps showing the homogenous distribution of Ni, Co, and Mn in the nanoneedle structure anchored on the VG surface. f) Capacitance retentions of different samples as a function of current density. (reproduced with permission from Ref. [9]; copyright 2015, Royal Society of Chemistry). g) Schematic illustration of the electron contact point on horizontal graphene and VG. h) Nyquist plots of No-CC, Foil-CC, Foam-CC, and VG/Foam-CC working electrodes. (reproduced with permission from Ref. [60]; copyright 2013, Wiley-VCH).

that has been reported for a metal oxide/hydroxide-based electrode, and asymmetric supercapacitor devices based on such electrodes also showed excellent energy and power densities (Figure 9c).^[10] In another study, multi-component Ni–Co–Mn hydroxide nanoneedles were prepared on a VG surface, forming a unique “nanoneedle-on-petal” structure (Figure 9d),^[9] where the Ni, Co, and Mn elements were homogeneously distributed within the nanoneedle structure (Figure 9e). Notably, such VG nanotemplates remarkably facilitated charge transfer, resulting in an ultrahigh rate capability of the hybrid electrodes, with a high capacitance retention up to 95% at the current density of 100 mA cm^{-2} , much higher than that of VG-free electrodes (Figure 9f).

Moreover, VG can act as a “bridge” between pseudocapacitive materials and current collectors, and provide quick channels for electron transfer. Such bridging effects have been systematically investigated by Bo *et al.*^[60] As schematically shown in Figure 9g, due to the surface roughness of both the current collector and the active materials, there were only a very limited number of contact points at the interface; yet the dense, exposed edges of VG could provide abundant pathways for charge transport. Moreover, the introduction of VG bridges on a nickel-foam current collector greatly reduced the constriction/spreading resistance caused by the limited contact points at the active layer/current collector interface. As a result, VG-bridged supercapacitors exhibited a much reduced interfacial resistance (Figure 9h) and markedly improved rate capa-

bility and cyclic stability. Indeed, such a “bridge” functionality has been widely observed in VG-based hybrid supercapacitor electrodes with significantly enhanced rate capability and structural stability.^[61,62] In addition to metal oxide/hydroxides, metal nitrides^[63] and conducting polymer^[64] have also been loaded on the VG surface as high-performance pseudocapacitive electrodes.

5.1.3. Microsupercapacitors

The rapid development of miniaturized portable electronic devices in modern life has driven an increasing demand for micro-power sources and micro-energy storage units.^[65] Among them, micro-supercapacitors have been attracting considerable attention, because of their high power density, desirable rate capability, and outstanding cyclic stability.

High-power micro-supercapacitors have been fabricated, consisting of an insulating substrate, an interdigitated VG electrode, and a Ti/Au current collector (Figure 10a).^[66] The VG microelectrodes were several micrometers in thickness (Figure 10b) and the as-prepared micro-supercapacitors exhibited a perfect capacitive behavior at scan rates up to 100 V s^{-1} (Figure 10c, 1000 times faster than conventional supercapacitors), a maximum power density of 292 W cm^{-3} at a current of 100 mA (Figure 10d), and excellent cycling stability. Moreover, it has been demonstrated that the design of the VG micro-electrode plays an essential role in determining the performance of the final micro-supercapacitor devices. In a study that

combined theoretical simulations and experimental studies, Chen *et al.*^[41] found that the electrical field distribution above the substrate material played a key role in the graphene coverage during micropattern fabrication. Figure 10e shows the electrical field at 50 nm above the substrate. It can be seen that the electric field above the gold stripe, especially near the edges (with even smaller radii of curvature) of the gold stripe was much higher than that above SiO_2 . As a result, the gases were ionized more efficiently above the gold stripe during the growth process, leading to preferential production of VG on the Au surface after the introduction of carbon precursors (Figure 10f). Indeed, the VG patterns can thus be controlled by manipulating the surface electric field distribution. Subsequently, a “selective-growth” method was proposed for the fabrication of CNT-VG micro-supercapacitors.^[67] Due to the high binding energy of carbon atoms absorbed on the CNT surface, VG prefers to grow on the CNT surface, rather than on the SiO_2 substrate, resulting in the formation of gaps (VG-free zone) between adjacent electrodes (Figure 10g-h). The as-prepared VG/CNT based micro-supercapacitors exhibit an ultrahigh areal capacitance of approximately 110 mF cm^{-2} at a current density of 0.3 mA cm^{-2} , outstanding long-term cycling stability (only $\approx 7\%$ loss of the initial capacitance after 10000 cycles), high thermal stability and high functional flexibility. The selective growth of VG on CNT patterns provides a novel technique for micro-supercapacitor fabrication with highly controllable gap width and high utilization efficiency of electrode materials along the axial direction, which is difficult to achieve by the conventional multistep micro-supercapacitor fabrication approaches.

In short, micro-supercapacitors based on VG has shown an ultrahigh power density, fast frequency response, and excellent long-term cyclability, since VG arrays display a high density of ordered alignment of few-layer graphene nanosheets, edge-enriched structure, open channels, and high electrical conductivity.^[68,69] Further investigations will focus on the manipulation of surface plasma and electrical field during the preparation of VG-microelectrodes, to realize the controllable and cost-effective fabrication of micro-supercapacitor devices.

In addition, VG grown on select current collectors (e.g., carbon cloth, Ni foam, etc.) can be used directly as free-standing electrodes without any binder or conductive additives, exhibiting high electrical conductivity and stability during electrochemical applications. To further increase the capacity and working voltage, it is critical to develop strategies whereby VG can be effectively and synergistically combined with other pseudocapacitive materials to produce high-performance electrodes.

5.2. Lithium-Ion Batteries

Secondary batteries, particularly lithium-ion battery (LIB), have been attracting extensive attention in both academic research and commercial applications, due to their high energy density, wide working-voltage window, and relatively long cycle life.^[67,70] Although widely used in portable electronic devices, some

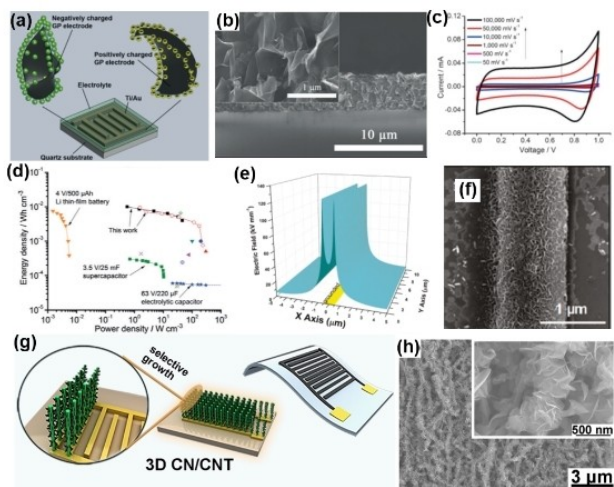


Figure 10. a) Scheme of a microsupercapacitor consisting of an insulating substrate, interdigitated VG electrodes, and Ti/Au current collectors. b) SEM image of the cross-section of a VG microelectrode. Inset is an enlarged SEM image. c) CV curves of microsupercapacitor devices at different scan rates. d) Ragone plot of the as-prepared VG-based microsupercapacitor in comparison to other contemporary devices. (reproduced with permission from Ref. [66]; copyright 2014, Wiley-VCH). e) Electric field distribution at 50 nm above the substrate surface of case I. The $1 \mu\text{m}$ -wide gold stripe is grounded ($V = 0$). f) VG grown on a single gold stripe in 2 min. (reproduced with permission from Ref. [41]; copyright 2011, American Chemical Society). g) Schematic picture of the formation of a VG/CNT microsupercapacitor. h) Uniform coverage of VG on CNT arrays. Inset shows the sharp edges of VG. (reproduced with permission from Ref. [67]; copyright 2019, Elsevier).

critical issues remain with LIB, e.g., low rate performance, poor cyclic stability, and safety problems,^[71–73] that limit the development in the commercial market of electrical vehicles.^[7] The key to high energy-density LIB with a long cycle life and good safety is the development of high-performance electrodes (anodes and cathodes) that can improve the performance of LIB to meet the increasing demand for energy in modern life.^[6,74,75]

Graphite has been widely used as the anode material for commercialized LIB, due to its low and flat working potential, long cycle life, and low cost. However, the lithium storage performance of graphite is limited, in terms of energy and power densities, due to the low theoretical capacity (LiC_6 , 372 mAh g^{-1}) and low Li-ion transport rate ($10^{-12} \sim 10^{-14} \text{ cm}^2 \text{ s}^{-1}$). As a unique derivative of carbon, graphene has attracted much attention as LIB anodes, with its high electrical conductivity, large specific surface area, and high mechanical strength.^[76] Moreover, it has been shown that graphene edges can significantly affect the reactivity of the carbon material toward the adsorption as well as the diffusion of Li ions.^[77] VG with abundant sharp edges can provide active sites for Li-ion insertion and extraction as well as fast electron transfer channels, showing great potential as high-performance LIB anodes. For instance, Xiao *et al.*^[78] directly prepared VG nanosheets on a current collector as binder-free LIB anodes, effectively facilitating both electron and lithium-ion transport and improving the rate capability. They demonstrated that the vertical alignment with an effective electrical connection to the substrate was beneficial to minimize electrical resistance. Subsequently, Cheng *et al.*^[79] investigated the effect of deposition time of VG on the electrochemical performance of VG anodes, and found that prolonging the deposition time of VG effectively increased the specific surface area of the graphene nanowalls, and thereby improved the performance of coin-type lithium-ion cells.^[79]

However, bare VG as LIB anodes still suffers low capacity, which cannot meet the requirement for practical applications. Great efforts have therefore been devoted to the design of VG-based composite anodes to enhance lithium-ion storage performance. Coating of VG nanosheets on Si particles^[80] or commercial SiO microparticles was found to provide a stable conducting network through interconnected VG encapsulation during lithiation, and remarkably improve the cycling stability of high mass-loading SiO anodes (Figure 11a).^[81] The macroscopic conductivity of the electrodes was then assessed by quantifying the sheet resistance of the composite electrodes on an insulating polyimide (PI) film. As shown in Figure 11b, the sheet resistance of the SiO@VG electrode ($\sim 200 \Omega/\text{sq}$) was much lower than those of SiO ($\sim 2200 \Omega/\text{sq}$) and SiO@horizontal graphene-based electrodes ($\sim 700 \Omega/\text{sq}$). As a result, a full LIB based on SiO@VG anode exhibited outstanding cycling stability ($\sim 80\%$ retention over 400 cycles) at a charge/discharge rate of 0.5 C/1 C (Figure 11c). Furthermore, 3D VG@SiO_x/B-doped carbon (3DVG@SiO_x/BC) composite electrodes were prepared with a high lithium-ion diffusion coefficient ($1.7 \times 10^{-9} \text{ cm}^2 \text{ s}^{-1}$) and an ultralow volume change (13.8%).^[82] Consequently, a full cell with such a composite anode and LiCoO₂ cathode showed a high gravimetric and volumetric energy density of

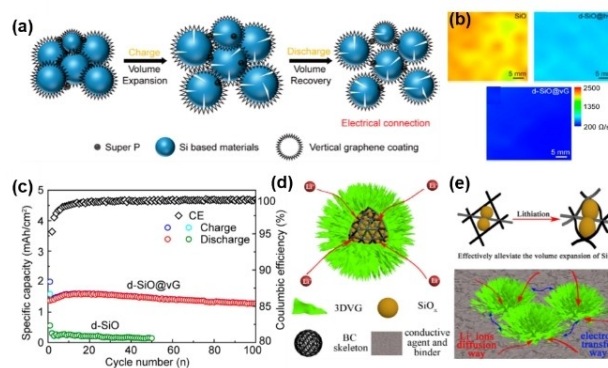


Figure 11. a) Scheme of the functional mechanism of VG coating on Si-based materials during the charge/discharge process. b) 2D mapping images of the sheet resistance of SiO, d-SiO@horizontal graphene, and d-SiO@VG composite electrodes on a PI film. c) Cyclic stability of d-SiO and d-SiO@VG electrodes at a current density of 320 mA g^{-1} . (reproduced with permission from Ref. [81]; copyright 2017, American Chemical Society). d, e) Schematic illustrations of the lithium-ion storage mechanism of the 3D VG@SiO_x/BC electrode. (reproduced with permission from Ref. [82]; copyright 2020, Wiley-VCH).

459.4 Wh kg^{-1} and 1167.9 Wh L^{-1} , respectively. The excellent electrochemical performance was attributed to the combination of uniformly dispersed sub-nanoscale black carbon (BC) and a 3D VG coating layer on the surface of SiO_x spheres to form a 3D conductive and robust network, which supplied a fast transport path for Li ions and effectively suppressed the volume change of SiO_x (Figure 11d-e).^[82]

Besides SiO_x-based anodes, Yang *et al.*^[83] employed VG as substrates to load MoS₂ nanosheets as a hybrid LIB anode. Compared with MoS₂/carbon black, MoS₂/VG nanocomposites exhibited an enhanced electrochemical performance, delivering a specific capacity of 1277 mAh g^{-1} at a current density of 100 mA g^{-1} and a high first-cycle coulombic efficiency of 76.6%. The MoS₂/VG nanostructures also retained a high capacity of 1109 mAh g^{-1} after 100 cycles at a current density of 200 mA g^{-1} , indicating outstanding cyclic stability.^[83] Moreover, Rawat *et al.* prepared MoS₂ on a VG foam and planar graphene foam respectively, and compared their electrochemical properties. The MoS₂@VG electrodes exhibited an improved capacity of 670 mAh g^{-1} with 99% capacity retention after 30 cycles at 100 mA g^{-1} , much better than that of MoS₂@planar graphene electrodes (only 550 mAh g^{-1} at 100 mA g^{-1}). Such a superior performance of the VG-based electrode was attributed to the unique hierarchical structure and densely packed reactive edges of VG.^[84]

In fact, for LIB anode design, VG is widely used as a scaffold for active materials forming 3D structures to enhance structural stability and alleviate volume change. For instance, a 3D free-standing electrode based on a VG foam loaded with oriented TiO₂ nanosheets (Figure 12a) for LIB was designed and exhibited a high discharge capacity and extremely long cycling stability that after testing at 8 C over 12000 cycles, the capacity of the cell retained 82% of the initial state, and when the current density was scaled back to 2 C, the cell still delivered high capacity retention of over 86% (Figure 12b).^[85] Such cycling

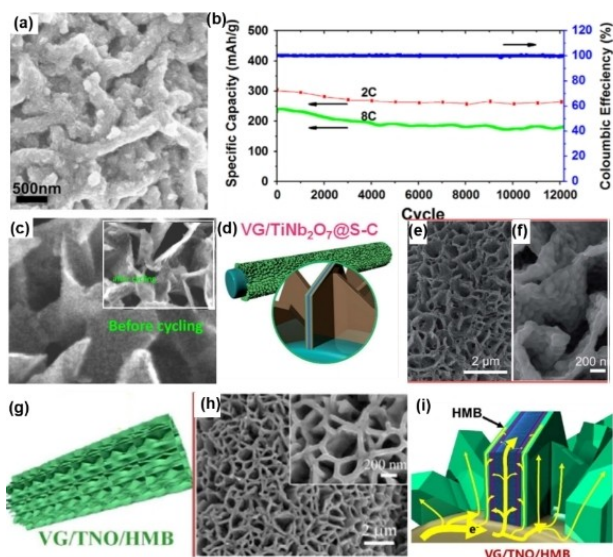


Figure 12. a) SEM of TiO_2 nanosheets on a VG foam. b) Cycling stability of TiO_2/VG foam at continuous cycling at 2.67 A g^{-1} (8 C) and sampling at 0.66 A g^{-1} (2 C). (reproduced with permission from Ref. [85]; copyright 2016, Elsevier). c) SEM images of a ZnO/VG electrode before and (inset) after cycling. (reproduced with permission from Ref. [86]; copyright 2014, American Chemical Society). d) Schematic of the formation process of $\text{VG}/\text{TiNb}_2\text{O}_7@\text{S-C}$ core/shell arrays. e, f) SEM images of $\text{VG}/\text{TiNb}_2\text{O}_7@\text{S-C}$ core/shell structure. (reproduced with permission from Ref. [87]; copyright 2018, Royal Society of Chemistry). g) Scheme of the $\text{VG}/\text{TNO}/\text{HMB}$ core/shell structure. h) SEM image of $\text{VG}/\text{TNO}/\text{HMB}$ core/shell arrays. Inset is a magnified image. i) Schematic illustration of electron transfer in the $\text{VG}/\text{TNO}/\text{HMB}$ structure. (reproduced with permission from Ref. [88]; copyright 2018, Elsevier).

stability was much better than that of many state-of-the-art TiO_2 -based LIB anodes, likely because VG with sharp edges contributed to dense nucleation and growth of TiO_2 nanosheets, which provided effective channels for electrolyte ions, facile access of the sheet surface, and thin sheets for a reduced Li^+ transport path.^[85] Besides TiO_2 , high-performance binder-free ZnO/VG hybrid anodes have also been fabricated by anchoring ZnO nanoparticles on VG through a facile hydrothermal process (Figure 12c).^[86] In such a hybrid structure, the good conductivity of VG and the ultrasmall size of ZnO particles were beneficial to the completely reversible electrochemical reaction of anodes, resulting in high structural stability and long cycle life (Figure 12c inset).

Moreover, highly conductive networks introduced on VG-based structures can further improve the electrochemical performance of the composite anodes. Recently, a hierarchical structure with a $\text{VG}/\text{TiNb}_2\text{O}_7/\text{S}$ -doped carbon (S-C) shell was prepared as a LIB anode, where VG and S-C worked cooperatively to establish a conductive network on TiNb_2O_7 through internal and external integration (Figure 12d–f).^[87] Notably, the hybrid electrode shows an excellent rate performance at medium-high temperatures ranging from 25 to 70°C . Similarly, in a “core-shell” electrode with hydrogen molybdenum bronze (HMB)/titanium niobium oxide ($\text{Ti}_2\text{Nb}_{10}\text{O}_{29}$, TNO)/VG (Figure 12g–h),^[88] VG and HMB served as powerful conductive “body guards” for the TNO guest with enhanced conductivity and reinforced structural stability (Figure 12i). Consequently,

the $\text{VG}/\text{TNO}/\text{HMB}$ anode showed high capacities (317 mAh g^{-1} at 2 C, and 163 mAh g^{-1} at 60 C), excellent cycling life, and superior high-rate capability.

In summary, for LIB applications, VG with sharp edges can provide numerous active sites and fast channels for electron/ion transfer, but VG itself shows limited lithium storage. With high-capacity materials coated on VG, the capacitive performance of the electrodes can be significantly enhanced. Yet the concurrent increase of the overall electrode mass results in a reduced energy density. Further research is desired to address this dilemma.

5.3. Lithium-Metal Batteries

Recently, high energy-density Li metal anodes have been widely investigated, because of their irreplaceable position in the development of “next-generation” rechargeable batteries, such as Li-air and Li-S batteries.^[89,90] However, safety issues remain, which originate from the formation of Li dendrites as well as unstable solid electrolyte interphase.^[91,92] Therefore, VG has been proposed as an effective scaffold for lithium metal to form composite electrodes to mitigate these issues. Peng *et al.* investigated the Li plating behaviors using an electrode of VG grown on Ni foam (VG/Ni).^[93] Such a hybrid structure exhibited a significant pseudocapacitive interfacial feature, greatly improved Li^+ transfer kinetics, and uniform Li plating/stripping for stable Li metal cycling (Figure 13a) even at a high depth of discharge of 50%. In another study,^[94] a composite electrode based on $\text{Si}@\text{VG}$ arrays-supported lithium was prepared through a simple melt infusion process (Figure 13b). According to the simulation results (Figure 13c), the current density of the internal interface of the VG structure was larger than those of other areas, indicating that Li-ion flux was preferentially deposited into the porous structure of the VG substrate rather

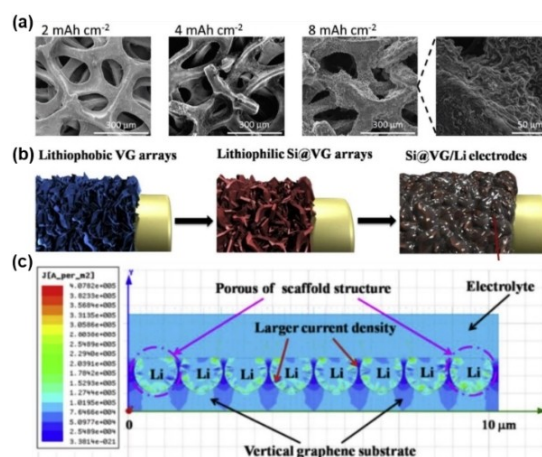


Figure 13. a) Top surface morphologies of Li plating at 2, 4, 8 mAh cm^{-2} on VG/Ni (reproduced with permission from Ref. [93]; copyright 2018, Wiley-VCH). b) Schematic illustrations of the melt-infusion process of $\text{Si}@\text{VG}$ arrays. c) Simulation and calculation results of the current density between the electrolyte and $\text{Si}@\text{VG}/\text{Li}$ electrode. (reproduced with permission from Ref. [94]; copyright 2018, Elsevier).

than onto the external surface of the VG arrays. Additionally, the porous VG scaffold structure could alleviate the volume expansion and inhibit the formation of dendritic lithium significantly, leading to excellent cyclic stability of the Li composite anode.

Notably, in lithium-metal battery applications, a range of interfacial issues have been found between the lithium metal and solid-state electrolytes that limit the device performance,^[95] such as poor contact, growth of lithium dendrites, structural instability, etc. These may be mitigated by deliberate structural engineering of VG, which is the focus of ongoing research.

5.4. Other Secondary Batteries

Compared to LIB, sodium-ion battery (SIB) shows great promise in large-scale industrial applications, due to similar chemical/physical properties of Na to Li, but significantly reduced cost and abundant resources.^[96] In recent years, exploring and designing novel electrode materials for high-performance SIB has become a research hotspot.^[97] VG-based structures have been demonstrated to effectively improve the electrochemical performance of SIB electrodes. Tu *et al.* designed a hierarchical structure with wrinkled MoSe₂ nanosheets sandwiched by a VG core and a N-doped carbon (N-C) shell (Figure 14a).^[98] Such a sandwiched core/shell array showed multiple benefits, including omni-bearing conductive networks from interconnected VG arrays and N-C layers (Figure 14b), structural protection, suppression of active materials loss from the N-C shell, as well as large porosity. Consequently, the VG/MoSe₂/NC anode exhibited a high capacity (540 mAh g⁻¹), enhanced rate capability (Figure 14c), and long-term cycling stability (298 mAh g⁻¹

at 2.0 A g⁻¹ after 1000 cycles).^[98] Similarly, a free-standing composite electrode based on hydrogen molybdenum bronze (HMB) sandwiched between a VG skeleton and a poly(3,4-ethylene dioxythiophene) (PEDOT) shell was prepared (Figure 14d), and showed improved rate capability and cyclic stability (Figure 14e-f).^[99] These results suggest that the design of hierarchical structures with a conductive coating on the active materials is an effective way to further improve the electrochemical properties of VG-based SIB electrodes. Additionally, tailoring VG with a special morphology and large porosity is critical in developing high-capacity and fast rate-response SIB. Fan *et al.*^[100] prepared VG on CuO nanowires forming a hierarchical VG-based nanotube structure (Figure 14g), and active materials could be further loaded on the VG surface. The resultant VG nanotube framework was demonstrated to deliver a high capacity and excellent high-rate long-term cyclability (Figure 14h-i), due to the unique hierarchical architecture.^[100]

In another study, nitrogen and phosphorus dual-doped vertical graphene (N,P-VG) was uniformly grown on carbon cloth (N,P-VG@CC) as a binder-free anode for flexible potassium ion battery (PIB).^[101] With the combined advantages of rich active sites, highly accessible surface, highly conductive network, large interlayer spacing, as well as robust structural stability, this anode exhibited a high capacity (344.3 mAh g⁻¹), excellent rate capability (2000 mA g⁻¹; 46.5% capacity retention), and prominent long-term cycling stability (82% capacity retention after 1000 cycles), outperforming most of the recently reported carbonaceous anodes. Moreover, VG has also been proposed as nanotemplates for V₂O₅ for high-performance zinc ion battery (ZIB).^[102] In such a hybrid structure, VG provided fast channels for electron transfer and large accessible surface area to the electrolyte, and acted as a bridge between the V₂O₅ nanosheets and current collector, offering a sufficient room for volume change. As a result, the V₂O₅/VG cathodes exhibited significantly improved rate capability and cyclic stability.

In short, similar to the application in LIB, VG is usually combined with other active materials to form hybrid electrodes so as to enhance the capacity in these secondary battery systems. The rational design of a hierarchical structure based on VG plays an essential role in achieving a high device performance.

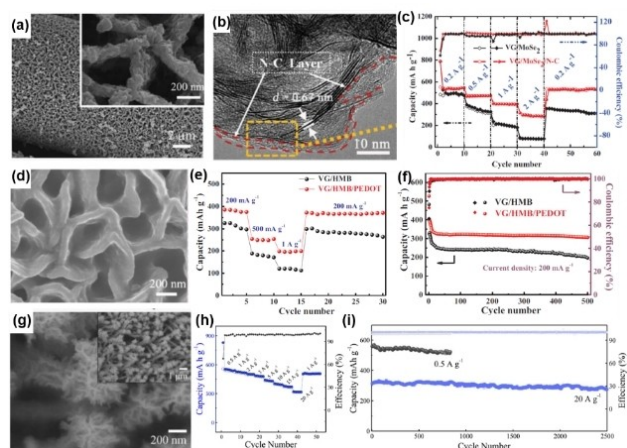


Figure 14. a) SEM image of VG/MoSe₂/N-C core/shell arrays. Inset is an enlarged SEM image. b) TEM image of the ternary sandwiched VG/MoSe₂/N-C core/shell arrays. c) Rate capability of VG/MoSe₂/N-C and VG/MoSe₂ electrodes. (reproduced with permission from Ref. [98]; copyright 2017, Wiley-VCH). d) SEM image of VG/HMB/PEDOT arrays. e) Rate capability of VG/HMB/PEDOT and VG/HMB electrodes. f) Cyclic stability of VG/HMB/PEDOT and VG/HMB electrodes. (reproduced with permission from Ref. [99]; copyright 2018, Elsevier). g) SEM images of a free-standing VG nanotube array. h) Rate capability of hierarchical VG nanotubes. i) Cyclic stability of hierarchical VG nanotubes. (reproduced with permission from Ref. [100]; copyright 2019, Elsevier).

5.5. Modification of Current Collectors

For the design of high-performance batteries, the current collector/electrode interfaces have also attracted extensive attention, due to their essential role in facilitating charge transport and achieving a high rate and good durability. Although traditional current collectors, such as Cu and Al foils, have been widely used in secondary batteries, they usually lack strong adhesion with the active materials, which compromises the interfacial conductivity and electrode stability and limits the rate capability of the batteries. Thus, modification strategies by VG decoration onto the current collectors have been developed to address such interfacial issues. Zhang *et al.*^[103] compared the

electrochemical properties of bare Cu (BC), VG coating Cu (VG), and commercial carbon-coated Cu (CC) current collectors in LIB (Figure 15a–c). As shown in Figure 15d, the main interfacial contact area of copper could be classified into the interfaces of copper/active material and copper/conductive material/adhesive. However, for both VG and CC, copper was always in contact with carbon. Since the wetting property of Cu on carbon (referred to as graphite anode materials) was inferior to that of carbon (e.g., amorphous carbon and graphene) on carbon, the interface in BC contained a lower contact area with active materials than VG and CC. After several cycles, a solid electrolyte interface film was generated at the interfaces (Figure 15e). For carbon-coated copper foils (VG and CC), the increasing contact surface area between the active materials and current collectors decreased the interfacial resistance, and for VG-coated Cu, a stable low-resistance solid electrolyte interface film was formed instead.^[103] As a result, VG-coated Cu exhibited an enhanced rate performance at high current densities (Figure 15f) and excellent cyclic stability (Figure 15g).

Peng *et al.*^[104] demonstrated that VG nanosheets grown on a commercial Al foil (VG–Al) formed a robust connection with the carbon-based conductive network of the electrode, thereby significantly reducing the electrode/current collector interfacial resistance. For Al current collectors, due to the relatively smooth surface and weak interaction between alumina, the polar native oxide layer on the Al surface, and the non-polar conductive carbon black, the contact sites between the Al foil and electrodes were limited, resulting in a high interfacial resistance and severely hindering interfacial charge transfer. In sharp contrast, VG with a large specific surface area on the VG–Al surface possessed abundant contacting sites with the

electrode, providing microscopic conductive paths at the electrode/current collector interface. Furthermore, VG nanosheets and carbon black, which are both non-polar sp^2 carbon materials, can be tightly connected through strong π - π interactions. At the interface between the electrode and VG–Al, carbon black nanoparticles were indeed found to be spread evenly on the VG nanosheets, which indicated that the conductive network in the electrode was in tight contact with the current collector, resulting in a low interfacial resistance.^[104]

6. Conclusions and Outlook

The intrinsic structures and outstanding properties of VG have significantly widened the applications of graphene materials in various advanced technologies. VG nanosheets can be grown by plasma-enhanced CVD methods featuring a vertical orientation, sharp edges, few-layer thickness, and open network channels, and show great potential as effective electrode materials for important electrochemical energy technologies. Mechanistically, it is believed that the vertical growth of VG is based on a defect-derived nucleation process and is significantly influenced by the electric field, internal stress, and anisotropic growth effect. Compared to conventional horizontal graphene, VG shows a large accessible surface area with resistance against aggregation and numerous exposed thin edges that provide abundant active sites for ion/charge absorption/desorption in electrochemical reactions. VG nanosheets can also act as strengthening ribs, remarkably improving the mechanical strength of the electrodes. These outstanding properties make VG promising as both an active material and nanotemplate for electrochemical energy storage systems. The electrochemical performance of VG-based electrodes can be further improved by deliberate structural engineering, such as doping, surface treatment, nanoengineering, active-material loading, and conductive-network construction.

Nevertheless, whereas substantial progress has been achieved in the development of VG-based electrodes for supercapacitors and LIB, the applications of VG for other novel multivalent-ion battery systems have been rarely reported. In fact, as compared to conventional graphene materials, the potential of VG has not been fully exploited, in particular, in light of recent research progress where VG has been found to exhibit highly active sites for catalysis and sensing.^[105,106] Several critical issues emerge in the further development of VG-based functional materials for electrochemical energy storage technologies:

(1) High cost and low yield of VG. The area and mass of VG produced so far are severely limited due to the restriction of plasma-based synthesis methods. Moreover, high-cost equipment and maintenance hinder the further development of VG in industrial applications. Meanwhile, the relationship between experimental parameters (e.g., plasma source, plasma power, gas source, growth time, etc.) and VG microstructures needs to be carefully examined to establish a fundamental framework for structural engineering of VG (e.g., graphene interlayer, defect, lateral size, etc.).

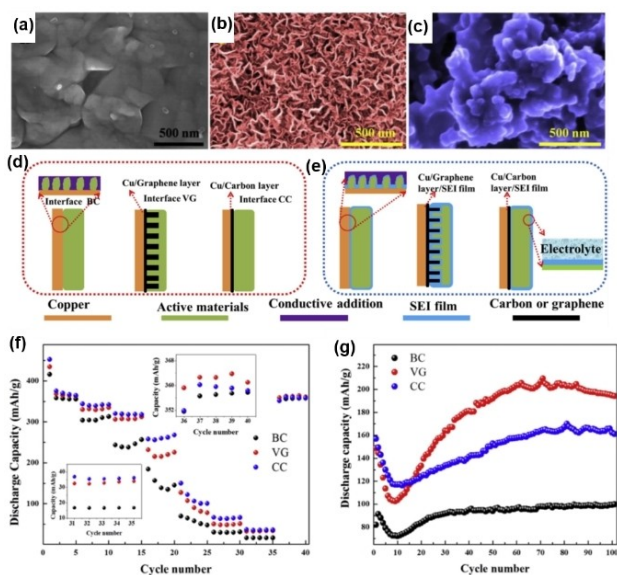


Figure 15. SEM images of different anode surfaces: a) BC, b) VG, and c) CC. Schemes of d) various interfaces of anodes using BC, VG, and CC as the current collector, the left denotes the BC interface, the right represents the CC interface and the middle is the VG interface, and e) the interface after several cycles. f) Rate performance of BC, VG, and CC at 0.1, 0.2, 0.3, 0.5, 1, 3, 5, and 0.1 C; g) discharge capacity of BC, VG, and CC in 100 cycles at 3 C. (reproduced with permission from Ref. [103]; copyright 2018, Elsevier).

(2) Low usage efficiency of VG in hybrid electrodes. VG-based composites are expected to show extraordinary properties, due to the synergistic effects between VG and other components. However, the introduction of VG into the hybrid electrodes inevitably increases the total mass and thus decreases the energy density. Thus, to achieve high-performance VG-based energy devices, it is critical to make the best use of the high conductivity and large surface area of VG in the composite electrodes.

(3) Limited understanding of the growth and energy storage mechanism of VG. Although various theories have been proposed to account for the growth mechanism of VG, clear and direct evidence has been lacking. Moreover, in-depth investigation of the energy storage mechanism in VG-based electrodes has been mostly neglected in research work.

To mitigate these issues, further research is desired with a focus on the following areas:

(1) Scale-up production of VG. A deep understanding of the plasm-based CVD techniques and customized instrumentation are required for the large-scale fabrication of VG at reduced cost, where roll-to-roll manufacturing and multi-linear antenna microwave plasma-assisted methods are viable technologies.^[107] Moreover, novel liquid-/solid-state precursors are needed to further reduce the production cost and improve safety during the fabrication process.

(2) Rational design of hierarchical structures. Whereas VG can be used as nanotemplates or modification layers for hybrid electrode materials, size matching between VG and other nanostructures should be taken into consideration in the structural design, as every component in the composite plays a significant role in dictating the performance. Moreover, surface modification and functionalization of VG is crucial to enhance the contact with other materials and thus improve the performance of the hybrid electrodes.

(3) Advanced in-situ characterization and modeling methods for mechanism investigation. Specifically, in-situ characterization can yield clear insights into the VG growth dynamics, as well as the energy storage mechanism of VG-based electrodes. This will be helpful in constructing relevant structural models for theoretical simulation. The correlation between the experimental and theoretical results can then be exploited for the establishment of an unambiguous fundamental framework within which the structure of the electrode materials can be systematically engineered for an optimal performance.

Acknowledgments

This work is supported in part by the US National Science Foundation (CHE-1900235 and CHE-2003685). P.G.H. acknowledges support from the Beijing Natural Science Foundation (2204086).

Conflict of Interest

The authors declare no conflict of interest.

Keywords: vertical graphene · growth mechanism · structure engineering · two-dimensional nanostructure · electrochemical energy storage

- [1] M. J. Allen, V. C. Tung, R. B. Kaner, *Chem. Rev.* **2010**, *110*, 132–145.
- [2] Q. Zhang, B. Zhang, Y. Yu, K. Zhao, P. He, B. Huang, *J. Mater. Sci.* **2018**, *53*, 528–537.
- [3] W. Choi, I. Lahiri, R. Seelaboyina, Y. S. Kang, *Crit. Rev. Solid State Mater. Sci.* **2010**, *35*, 52–71.
- [4] M. Pumera, *Energy Environ. Sci.* **2011**, *4*, 668–674.
- [5] C. Liu, Z. Yu, D. Neff, A. Zhamu, B. Z. Jang, *Nano Lett.* **2010**, *10*, 4863–4868.
- [6] P. He, K. Zhao, B. Huang, B. Zhang, Q. Huang, T. Chen, Q. Zhang, *J. Mater. Sci.* **2018**, *53*, 4482–4493.
- [7] G. Kucinskis, G. Bajars, J. Kleperis, *J. Power Sources* **2013**, *240*, 66–79.
- [8] K. Ostrikov, E. Neyts, M. Meyyappan, *Adv. Phys.* **2013**, *62*, 113–224.
- [9] G. Xiong, P. He, L. Liu, T. Chen, T. S. Fisher, *J. Mater. Chem. A* **2015**, *3*, 22940–22948.
- [10] G. Xiong, P. He, D. Wang, Q. Zhang, T. Chen, T. S. Fisher, *Adv. Funct. Mater.* **2016**, *26*, 5460–5470.
- [11] L. Zhang, Z. Sun, J. L. Qi, J. Shi, T. Hao, J. Feng, *Carbon* **2016**, *103*, 339–345.
- [12] M. S. Dresselhaus, G. Dresselhaus, A. Jorio, A. G. Souza Filho, R. Saito, *Carbon* **2002**, *40*, 2043–2061.
- [13] Z. Ni, H. Fan, Y. Feng, Z. Shen, B. Yang, Y. Wu, *J. Chem. Phys.* **2006**, *124*, 204703.
- [14] J. Rouzaud, A. Oberlin, C. Beny-Bassez, *Thin Solid Films* **1983**, *105*, 75–96.
- [15] V. Blank, V. Denisov, A. Kirichenko, B. Kulnitskiy, S. Y. Martushov, B. Mavrin, I. Perezhogin, *Nanotechnology* **2007**, *18*, 345601.
- [16] K. Davami, M. Shaygan, N. Kheirabi, J. Zhao, D. A. Kovalenko, M. H. Rummeli, J. Opitz, G. Cuniberti, J.-S. Lee, M. Meyyappan, *Carbon* **2014**, *72*, 372–380.
- [17] C. Casiraghi, S. Pisana, K. Novoselov, A. K. Geim, A. Ferrari, *Appl. Phys. Lett.* **2007**, *91*, 233108.
- [18] S. Ghosh, K. Ganesan, S. R. Polaki, T. Ravindran, N. G. Krishna, M. Kamruddin, A. K. Tyagi, *J. Raman Spectrosc.* **2014**, *45*, 642–649.
- [19] M. Hiramatsu, M. Hori, *Carbon nanowalls: synthesis and emerging applications*, Springer Science & Business Media, **2010**.
- [20] J. Wang, M. Zhu, R. Outlaw, X. Zhao, D. Manos, B. Holloway, V. Mammana, *Appl. Phys. Lett.* **2004**, *85*, 1265–1267.
- [21] Z. Bo, K. Yu, G. Lu, P. Wang, S. Mao, J. Chen, *Carbon* **2011**, *49*, 1849–1858.
- [22] J. R. Miller, R. Outlaw, B. Holloway, *Science* **2010**, *329*, 1637–1639.
- [23] G. Xiong, P. He, Z. Lyu, T. Chen, B. Huang, L. Chen, T. S. Fisher, *Nat. Commun.* **2018**, *9*, 790.
- [24] Q. Zhang, Y. Wang, B. Zhang, K. Zhao, P. He, B. Huang, *Carbon* **2018**, *127*, 449–458.
- [25] Y. Wu, P. Qiao, T. Chong, Z. Shen, *Adv. Mater.* **2002**, *14*, 64–67.
- [26] A. T. Chuang, B. O. Boskovic, J. Robertson, *Diamond Relat. Mater.* **2006**, *15*, 1103–1106.
- [27] M. Hiramatsu, K. Shiji, H. Amano, M. Hori, *Appl. Phys. Lett.* **2004**, *84*, 4708–4710.
- [28] M. Hiramatsu, M. Hori, *Jpn. J. Appl. Phys.* **2006**, *45*, 5522.
- [29] S. Kurita, A. Yoshimura, H. Kawamoto, T. Uchida, K. Kojima, M. Tachibana, P. Molina-Morales, H. Nakai, *J. Appl. Phys.* **2005**, *97*, 104320.
- [30] G. Sato, T. Morio, T. Kato, R. Hatakeyama, *Jpn. J. Appl. Phys.* **2006**, *45*, 5210.
- [31] T. Mori, M. Hiramatsu, K. Yamakawa, K. Takeda, M. Hori, *Diamond Relat. Mater.* **2008**, *17*, 1513–1517.
- [32] M. A. Lieberman, A. J. Lichtenberg, *Principles of plasma discharges and materials processing*, John Wiley & Sons, **2005**.
- [33] T. Mori, M. Hiramatsu, K. Yamakawa, K. Takeda, M. Hori, *Diamond Relat. Mater.* **2008**, *17*, 1513–1517.
- [34] Z. Bo, S. Mao, Z. J. Han, K. Cen, J. Chen, K. K. Ostrikov, *Chem. Soc. Rev.* **2015**, *44*, 2108–2121.
- [35] A. Malesevic, R. Vitchev, K. Schouteden, A. Volodin, L. Zhang, G. Van Tendeloo, A. Vanhulsel, C. Van Haesendonck, *Nanotechnology* **2008**, *19*, 305604.
- [36] M. Zhu, J. Wang, B. C. Holloway, R. Outlaw, X. Zhao, K. Hou, V. Shutthanandan, D. M. Manos, *Carbon* **2007**, *45*, 2229–2234.
- [37] J. H. Warner, F. Schaffel, M. Rummeli, A. Bachmatiuk, *Graphene: Fundamentals and emergent applications*, Newnes, **2012**.

- [38] G. Xiong, K. P. S. S. Hembram, D. N. Zakharov, R. G. Reifengerger, T. S. Fisher, *Diamond Relat. Mater.* **2012**, 27–28, 1–9.
- [39] J. Zhao, M. Shaygan, J. r. Eckert, M. Meyyappan, M. H. Rummeli, *Nano Lett.* **2014**, 14, 3064–3071.
- [40] S. Kondo, S. Kawai, W. Takeuchi, K. Yamakawa, S. Den, H. Kano, M. Hiramatsu, M. Hori, *J. Appl. Phys.* **2009**, 106, 094302.
- [41] K. Yu, P. Wang, G. Lu, K.-H. Chen, Z. Bo, J. Chen, *J. Phys. Chem. Lett.* **2011**, 2, 537–542.
- [42] L. L. Zhang, X. Zhai, *Chem. Soc. Rev.* **2009**, 38, 2520–2531.
- [43] B. E. Conway, *Electrochemical supercapacitors: scientific fundamentals and technological applications*, Springer Science & Business Media, **2013**.
- [44] Y. Zhang, Q. Zou, H. S. Hsu, S. Raina, Y. Xu, J. B. Kang, J. Chen, S. Deng, N. Xu, W. P. Kang, *ACS Appl. Mater. Interfaces* **2016**, 8, 7363–7369.
- [45] H. Yang, X. Zhang, J. Yang, Z. Bo, M. Hu, J. Yan, K. Cen, *J. Phys. Chem. Lett.* **2017**, 8, 153–160.
- [46] S. Ghosh, G. Sahoo, S. Polaki, N. G. Krishna, M. Kamruddin, T. Mathews, *J. Appl. Phys.* **2017**, 122, 214902.
- [47] G. Sahoo, S. Polaki, S. Ghosh, N. Krishna, M. Kamruddin, *J. Power Sources* **2018**, 401, 37–48.
- [48] Y.-W. Chi, C.-C. Hu, H.-H. Shen, K.-P. Huang, *Nano Lett.* **2016**, 16, 5719–5727.
- [49] S. R. Varanasi, S. K. Bhatia, *J. Phys. Chem. C* **2016**, 120, 27925–27933.
- [50] C. Lian, K. Liu, H. Liu, J. Wu, *J. Phys. Chem. C* **2017**, 121, 14066–14072.
- [51] H. Yang, Z. Bo, J. Yan, K. Cen, *Int. J. Heat Mass Transfer* **2019**, 133, 416–425.
- [52] Q. Z. Zhang, D. Zhang, Z. C. Miao, X. L. Zhang, S. L. Chou, *Small* **2018**, 14, 1702883.
- [53] G. Xiong, K. P. S. S. Hembram, R. Reifengerger, T. S. Fisher, *J. Power Sources* **2013**, 227, 254–259.
- [54] Z. Zhang, Y. Xiao, Y. Zhang, W. Zhang, *J. Nanosci. Nanotechnol.* **2019**, 19, 5864–5870.
- [55] N. Soin, S. S. Roy, S. K. Mitra, T. Thundat, J. A. McLaughlin, *J. Mater. Chem.* **2012**, 22, 14944–14950.
- [56] Q. Liao, N. Li, S. Jin, G. Yang, C. Wang, *ACS Nano* **2015**, 9, 5310–5317.
- [57] G. Sahoo, S. Polaki, N. Krishna, M. Kamruddin, *J. Phys. D* **2019**, 52, 375501.
- [58] G. Xiong, P. He, L. Liu, T. Chen, T. S. Fisher, *Front. Energy Res.* **2015**, 3, 39.
- [59] X. Wang, J. Liu, Y. Wang, C. Zhao, W. Zheng, *Mater. Res. Bull.* **2014**, 52, 89–95.
- [60] Z. Bo, W. Zhu, W. Ma, Z. Wen, X. Shuai, J. Chen, J. Yan, Z. Wang, K. Cen, X. Feng, *Adv. Mater.* **2013**, 25, 5799–5806.
- [61] P. He, Q. Zhang, Q. Huang, B. Huang, T. Chen, *RSC Adv.* **2018**, 8, 13891–13897.
- [62] P. He, B. Huang, Q. Huang, T. Chen, Q. Zhang, *J. Mater. Sci.* **2018**, 53, 12352–12364.
- [63] H. Qi, S. Yick, O. Francis, A. Murdock, T. van der Laan, K. K. Ostrikov, Z. Bo, Z. Han, A. Bendavid, *Energy Storage Mater.* **2020**, 26, 138–146.
- [64] G. Xiong, C. Meng, R. G. Reifengerger, P. P. Irazoqui, T. S. Fisher, *Adv. Energy Mater.* **2014**, 4, 1300515.
- [65] G. Xiong, P. He, B. Huang, T. Chen, Z. Bo, T. S. Fisher, *Nano Energy* **2017**, 38, 127–136.
- [66] G. Xiong, C. Meng, R. G. Reifengerger, P. P. Irazoqui, T. S. Fisher, *Energy Technol.* **2014**, 2, 897–905.
- [67] P. He, Z. Ding, X. Zhao, J. Liu, Q. Huang, J. Peng, L.-Z. Fan, *Carbon* **2019**, 155, 453–461.
- [68] D. Aradilla, M. Delaunay, S. Sadki, J.-M. Gérard, G. Bidan, *J. Mater. Chem. A* **2015**, 3, 19254–19262.
- [69] S. Zheng, Z. Li, Z.-S. Wu, Y. Dong, F. Zhou, S. Wang, Q. Fu, C. Sun, L. Guo, X. Bao, *ACS Nano* **2017**, 11, 4009–4016.
- [70] P. He, Z. Ding, X. Zhao, J. Liu, S. Yang, P. Gao, L.-Z. Fan, *Inorg. Chem.* **2019**, 58, 12724–12732.
- [71] T. Jiang, P. He, G. Wang, Y. Shen, C. W. Nan, L. Z. Fan, *Adv. Energy Mater.* **2020**, 10, 1903376.
- [72] J. Hu, P. He, B. Zhang, B. Wang, L.-Z. Fan, *Energy Storage Mater.* **2020**, 26, 283–289.
- [73] K. Liu, Y. Liu, D. Lin, A. Pei, Y. Cui, *Sci. Adv.* **2018**, 4, 9820.
- [74] C. Wu, X. Zeng, P. He, L. Chen, W. Wei, *Adv. Mater. Interfaces* **2018**, 5, 1701080.
- [75] L. Lu, X. Han, J. Li, J. Hua, M. Ouyang, *J. Power Sources* **2013**, 226, 272–288.
- [76] J. Hassoun, F. Bonaccorso, M. Agostini, M. Angelucci, M. G. Betti, R. Cingolani, M. Gemmi, C. Mariani, S. Panero, V. Pellegrini, *Nano Lett.* **2014**, 14, 4901–4906.
- [77] C. Uthaisar, V. Barone, *Nano Lett.* **2010**, 10, 2838–2842.
- [78] X. Xiao, P. Liu, J. S. Wang, M. Verbrugge, M. P. Balogh, *Electrochem. Commun.* **2011**, 13, 209–212.
- [79] Q. Yang, J. Wu, S. Li, L. Zhang, J. Fu, F. Huang, Q. Cheng, *Diamond Relat. Mater.* **2019**, 91, 54–63.
- [80] M. Han, Z. Lin, X. Ji, Y. Mu, J. Li, J. Yu, *Mater. Today* **2020**, 17, 100445.
- [81] L. Shi, C. Pang, S. Chen, M. Wang, K. Wang, Z. Tan, P. Gao, J. Ren, Y. Huang, H. Peng, *Nano Lett.* **2017**, 17, 3681–3687.
- [82] M. Han, J. Li, J. Yu, *Energy Technol.* **2020**, 8, 2000351.
- [83] Y. Xiao, B. Chen, D. H. Seo, Z. J. Han, J. I. Wong, K. K. Ostrikov, H. Zhang, H. Y. Yang, *NPG Asia Mater.* **2016**, 8, 268.
- [84] B. Ouyang, Y. Wang, Z. Zhang, R. Rawat, *Electrochim. Acta* **2016**, 194, 151–160.
- [85] G. Ren, M. N. F. Hoque, J. Liu, J. Warzywoda, Z. Fan, *Nano Energy* **2016**, 21, 162–171.
- [86] N. Li, S. Jin, Q. Liao, C. Wang, *ACS Appl. Mater. Interfaces* **2014**, 6, 20590–20596.
- [87] S. Shen, W. Guo, D. Xie, Y. Wang, S. Deng, Y. Zhong, X. Wang, X. Xia, J. Tu, *J. Mater. Chem. A* **2018**, 6, 20195–20204.
- [88] S. Deng, D. Chao, Y. Zhong, Y. Zeng, Z. Yao, J. Zhan, Y. Wang, X. Wang, X. Lu, X. Xia, *Energy Storage Mater.* **2018**, 12, 137–144.
- [89] T. S. Wang, X. Liu, X. Zhao, P. He, C. W. Nan, L. Z. Fan, *Adv. Funct. Mater.* **2020**, 30, 2000786.
- [90] D. Lin, Y. Liu, Y. Cui, *Nat. Nanotechnol.* **2017**, 12, 194.
- [91] X.-B. Cheng, R. Zhang, C.-Z. Zhao, Q. Zhang, *Chem. Rev.* **2017**, 117, 10403–10473.
- [92] J. Qian, W. A. Henderson, W. Xu, P. Bhattacharya, M. Engelhard, O. Borodin, J.-G. Zhang, *Nat. Commun.* **2015**, 6, 6362.
- [93] F. Ren, Z. Lu, H. Zhang, L. Huai, X. Chen, S. Wu, Z. Peng, D. Wang, J. Ye, *Adv. Funct. Mater.* **2018**, 28, 1805638.
- [94] Y. Zhang, S. Liu, X. Wang, Y. Zhong, X. Xia, J. Wu, J. Tu, *J. Power Sources* **2018**, 374, 205–210.
- [95] G. Wang, P. He, L. Z. Fan, *Adv. Funct. Mater.* **2020**, 2007198.
- [96] K. Chayambuka, G. Mulder, D. L. Danilov, P. H. Notten, *Adv. Energy Mater.* **2018**, 8, 1800079.
- [97] Q. Huang, P. He, L. Xiao, Y. Feng, J. Liu, Y. Yang, B. Huang, X. Cui, P. Wang, W. Wei, *ACS Appl. Mater. Interfaces* **2019**, 12, 2191–2198.
- [98] D. Xie, X. Xia, Y. Zhong, Y. Wang, D. Wang, X. Wang, J. Tu, *Adv. Energy Mater.* **2017**, 7, 1601804.
- [99] J. Zhan, S. Deng, Y. Zhong, Y. Wang, X. Wang, Y. Yu, X. Xia, J. Tu, *Nano Energy* **2018**, 44, 265–271.
- [100] B. Ouyang, D. Chao, G. Jia, Z. Zhang, H. J. Fan, R. S. Rawat, *Energy Storage Mater.* **2019**, 18, 462–469.
- [101] W. Qiu, H. Xiao, Y. Li, X. Lu, Y. Tong, *Small* **2019**, 15, 1901285.
- [102] X. Zhang, Y. Tang, P. He, Z. Zhang, T. Chen, *Carbon* **2021**, 172, 207–213.
- [103] X. Liu, D. Wang, B. Zhang, C. Luan, T. Qin, W. Zhang, D. Wang, X. Shi, T. Deng, W. Zheng, *Electrochim. Acta* **2018**, 268, 234–240.
- [104] K. Wang, C. Wang, H. Yang, X. Wang, F. Cao, Q. Wu, H. Peng, *Nano Res.* **2020**, 13, 1948–1954.
- [105] C. Xu, Z. Bo, S. Wu, Z. Wen, J. Chen, T. Luo, E. Lee, G. Xiong, R. Amal, A. T. Wee, J. Yan, *Sol. Energy* **2020**, 208, 379–387.
- [106] A. M. Sajad, A. Shohreh, A. Belford, R. Amir, S. Wu, H. Z. Jun, A. Mohsen, *Nano-Micro Lett.* **2020**, 12, 109.
- [107] Z. Bo, M. Su, H. Yang, S. Yang, J. Yan, K. Cen, *Rev. Sci. Instrum.* **2020**, 91, 076105.

Manuscript received: October 22, 2020
Revised manuscript received: December 25, 2020
Accepted manuscript online: December 28, 2020